Droplet formation of biological non-Newtonian fluid in T-junction generators. II. Model for final droplet volume prediction

Merve Marcali,[1] Xiaoming Chen,[1] Marc G. Aucoin,[2] and Carolyn L. Ren[1,*]
[1]*Department of Mechanical and Mechatronics Engineering, University of Waterloo, Waterloo, Ontario, Canada*
[2]*Department of Chemical Engineering, University of Waterloo, Waterloo, Ontario, Canada*

(Received 19 May 2021; accepted 30 December 2021; published 14 February 2022)

This work represents the second part of a two-part series on the dynamics of droplet formation in a T-junction generator under the squeezing regime when using solutions of red blood cells as the dispersed phase. Solutions containing red blood cells are non-Newtonian; however, these solutions do not behave in the same way as other non-Newtonian fluids currently described in the literature. Hence, available models do not capture nor predict important features useful for the design of T-junction microfluidic systems, including droplet volume. The formation of a red blood cell-containing droplet consists of three stages: a lag stage, a filling stage, and a necking stage, with the lag stage only observed in narrow dispersed phase channel setups. Unlike other shear-thinning fluids, thread elongation into the main channel at the end of the necking stage is not observed for red blood cell solutions. In this work, a model that predicts the final droplet volume of a red blood cell containing droplets in T-junction generators is presented. The model combines a detailed analysis of the geometrical shape of the droplet during the formation process, with force and Laplace pressure balances to obtain the penetration depth (b^*_{fill}) and the critical neck thickness ($2r^*_{\text{pinch}}$) of the droplet. The performance of the model was validated by comparing the operational parameters (droplet volume, the spacing between the droplet, and the generation frequency) with the experimental data across a range of the dimensionless parameters (flow rate ratios, continuous phase viscosities, and channel geometries).

DOI: 10.1103/PhysRevE.105.025106

I. INTRODUCTION

In the first part of this study [1], solutions with two different concentrations of red blood cells were examined in a T-junction droplet generator in the squeezing regime. These solutions were made by diluting a stock solution containing 10% (v/v) red blood cells with phosphate buffered saline. Unlike Newtonian fluids where the channel geometry is what primarily governs droplet formation in the squeezing regime, droplets containing red blood cells were influenced by a combination of channel geometry ($h^* = aspect\ ratio$, $\Lambda = width\ ratio$) and flow conditions (fluid viscosities and $\varphi = flow\ rate\ ratio$).

Video analysis showed that the droplet formation consisted of three stages: lag, filling and necking stages (see, Fig. 1). In other work using non-Newtonian fluids as the dispersed phase, an additional stretching phase was observed, where a thread elongated into the main channel before detachment [2–8]. However, with the droplets containing red blood cells, there was no obvious thread elongation, and the droplets immediately pinched off from the corner of the T junction at the end of the necking stage. In the lag stage, the interface of the droplets receded into the dispersed phase channel after the previous droplet detached. Nevertheless, the receding interface was only observed in the channel designs that had a lower width ratio, which also resulted in a longer lag stage and a larger spacing between droplets. In the filling stage, the interface penetrated the main channel and deformed. The deformed droplet presented a characteristic shape, similar to Newtonian fluid droplets [9], which, for the latter, has been used in the estimation of droplet volume. Thus, it may be possible to utilize a similar mathematical expression in our model, taking into consideration two key parameters: the penetration depth droplet (b^*_{fill}) and the critical neck thickness ($2r^*_{\text{pinch}}$). The penetration depth at the end of the filling stage is denoted as b^*_{fill}. In the necking stage, the neck thickness of the droplet ($2r^*_n$) reduces until reaching the critical neck thickness of the droplet ($2r^*_{\text{pinch}}$) right before pinch-off. Contribution of the necking stage to the final droplet volume was calculated by defining the shape of the droplet at this stage and the critical neck thickness of the droplet ($2r^*_{\text{pinch}}$) right before pinch-off. The analysis of two critical variables (b^*_{fill} and $2r^*_{\text{pinch}}$) helps the development of a mathematical model.

In this work, we develop a model that predicts the final droplet volume for droplets containing red blood cells, which may provide insights into the design of droplet generators for biomedical applications. To verify the capability of the model on predicting the droplet volume, a comparison analysis of the experimental data with the calculated data for all experiments was performed. (All the variables, parameters and equations are summarized in the Supplemental Material, S1 [10]).

II. MODEL

Scaling analysis of droplet volume for Newtonian fluids can be calculated as the given Eq. (1) below [11]:

$$V_d{}^* = \alpha_{\text{lag}} + \alpha_{\text{fill}} + \beta\varphi, \tag{1}$$

*c3ren@uwaterloo.ca

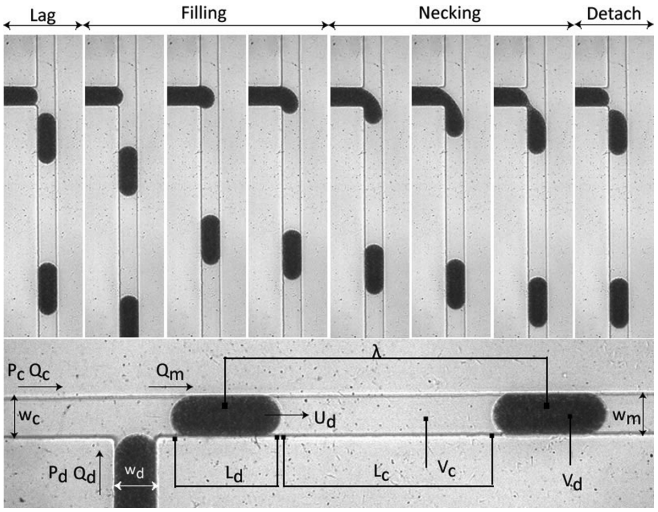

FIG. 1. Microscope images showing the formation cycle of a droplet containing red blood cells in a T-junction generator. The cycle starts with the lag stage and ends with the detachment of the droplet. Continuous phase flow rate $(Q_c) = 0.59$ μl/ min. Dispersed phase flow rate $(Q_d) = 0.30$ μl/min. Continuous phase capillary number (Ca) = 0.0099. Continuous phase channel width $(w_c) = 105$ μm. Dispersed phase channel width $(w_d) = 102$ μm. Main channel width $(w_m) = 105$ μm. Channel height $(h) = 62.9$ μm. The droplet length is denoted as L_d and its volume as V_d with a generation frequency f. Spacing between droplets is denoted as λ.

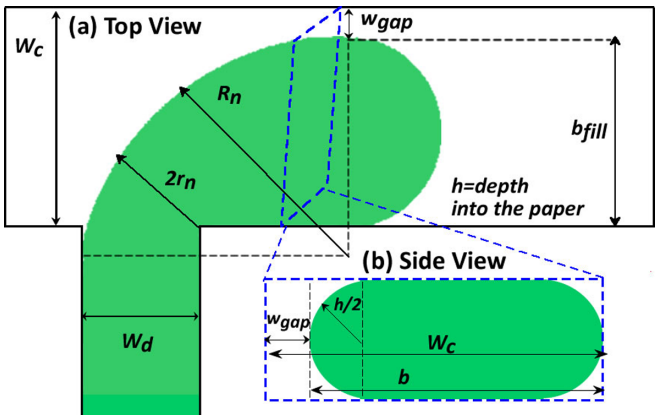

FIG. 2. Schematic of a 2D view of the characteristic shape of the droplet (a) view from the top (b) view from the cross-section area of the channel.

where φ is the flow rate ratio, α_{lag} and α_{fill} are the volumes added during the lag and filling stages, respectively, and β is the dimensionless necking time which relates to the growth of the droplet while the neck of the droplet collapses. For droplets containing red blood cells, the shear thinning property of the droplet impacted the filling and necking stages. Therefore, we aimed to develop a similar three-term model that accounted for the properties of the different dispersed phase, and to validate the model based on experimental data.

The mathematical expressions of these factors are related to the characteristic geometrical shape of the droplet which is defined by van Steijn *et al.* [9] as in Eq. (2):

$$V = hA - \frac{h^2}{2}\left(1 - \frac{\pi}{4}\right)l, \tag{2}$$

where h is the channel height, A is the projected area, and l is the perimeter of a droplet. Adapting the analysis to our system, certain requirements and assumptions were needed. First, the out of plane curvature of the droplet was assumed to be $h/2$, which is valid for good nonwetting conditions [12]. Second, all the droplets were pluglike, and the sizes were larger than the channel width. Third, any dynamic change in interfacial tension was neglected by avoiding the use of surfactant, and the interfacial tension was further assumed to be at equilibrium throughout the formation process [13,14]. Additional variables that defined our system (see, Fig. 2), included: the penetration of the droplet interface into the main channel, b_{fill}, which also defines the diameter of the half-circle at the front of the droplet; the back circle radius, R_n; and the distance from the droplet interface to the opposite corner of the T junction, $2r_n$. In the following sections, mathematical expressions for α_{lag}, α_{fill} and β factors expressed with respect to these variables are explained.

A. Lag stage

In this stage, the droplet interface receded into the dispersed phase channel after the detachment of the previous droplet. Then, the interface was pushed back to the entrance of the junction. The contribution of this recovery to the final droplet volume can be described based on the shape of the interface of the droplet after the previous droplet detaches (see, Fig. 3). By applying Eq. (2) to this shape, the lag phase volume α_{lag} can be calculated using the Eq. (3) given below:

$$V^*_{\text{lag}} = \alpha_{\text{lag}} = L^*_{\text{lag}}\Lambda + \frac{1}{2}\left(1 - \frac{\pi}{4}\right)\left(\Lambda^2 + \frac{\pi\Lambda h^*}{2}\right), \tag{3}$$

where α_{lag} is the dimensionless lag volume and L^*_{lag} is the dimensionless lag distance. The only unknown in this equation was the lag distance. Since the lag distance has an undefined and a complex relation with the flow conditions and the channel geometry, instead of defining a mathematical expression, we used experimental data and inserted it into Eq. (3) in the current model. Experimental observations showed that the lag distance occurred when a narrower dispersed phase channel was used. For wider channel designs, the droplet interface remained right at the junction after pinch-off the previous droplet and the lag distance became immeasurable ($L^*_{\text{lag}} \sim$ 1–2 μm) (see, Fig. 3). Thus, the contribution of the lag stage was considered only for the designs with $\Lambda = 0.5$, while calculating the final droplet volume.

B. Filling stage

In this stage, as the interface penetrates the main channel, the droplet interface is deformed and the viscous, pressure and interfacial tension forces determine the characteristic shape of the droplet [9,15]. For the droplets containing blood cells, the characteristic shape consisted of two small circular geometries (see, Fig. 4). The first one was a half circle located at the front of the droplet with a diameter b_{fill}, and the second one was a circular segment located at the back of the droplet with a radius R_n. Depending on the width

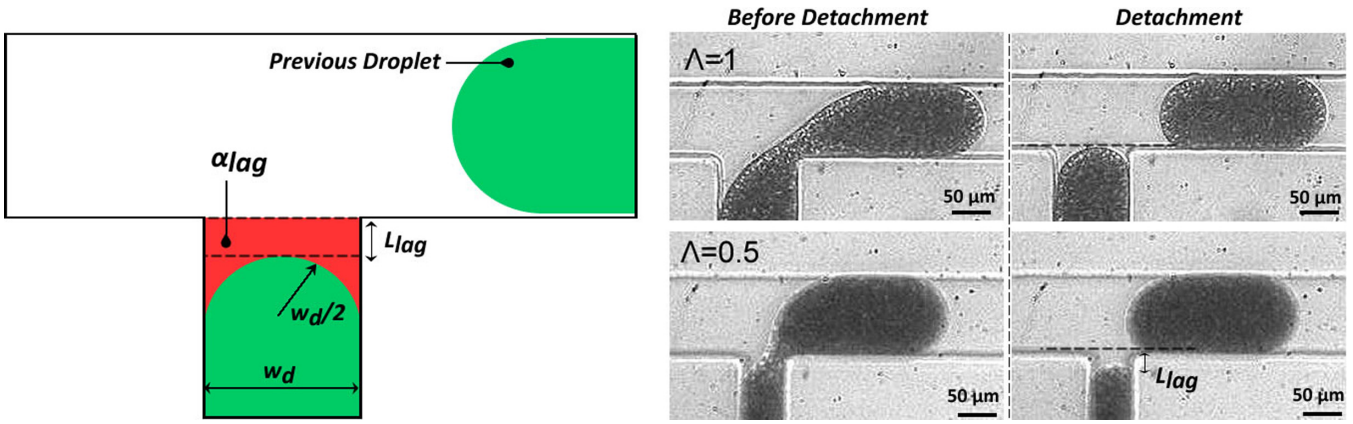

FIG. 3. Schematic of the droplet interface during the lag stage (on the left). Microscopic images of droplets of blood solutions before and after the detachment for two different channel width ratios (on the right).

ratio of the channel, the radius of the circular segment at the back was changing, and it became either equal to b_{fill} or w_d ($R_n = b_{\text{fill}}$; *if* $w_d \leqslant b_{\text{fill}}$ *or* $R_n = w_d$; *if* $w_d > b_{\text{fill}}$). Thus, two different cases defined the volume at the filling stage [see Figs. 4(a) and Fig. 4(b)]. Once Eq. (1) was applied to these geometries, the filling volume was defined for $w_d \leqslant b_{\text{fill}}$ as

$$V^*_{\text{fill}} = \alpha_{\text{fill}} = \frac{3}{8}\pi b^{*2}_{\text{fill}} - \frac{h^*}{2}\left(1-\frac{\pi}{4}\right)(\pi b^*_{\text{fill}} + (b^*_{\text{fill}} - \Lambda)). \quad (4)$$

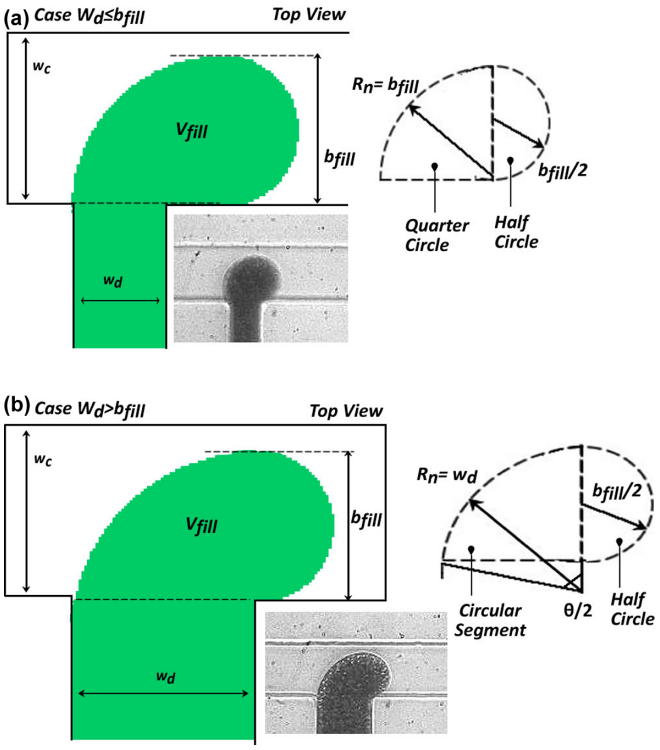

FIG. 4. Schematic of 2D shape of the droplet at the end of filling stage for two cases: (a) For cases where $w_d \leqslant b_{\text{fill}}$, the back half of the droplet is a quarter circle with diameter equal to b_{fill}; (b) For cases where $w_d > b_{\text{fill}}$, the radius of the circular segment equals the dispersed phase channel width.

In this case, the circular segment at the back was a quarter circle. However, for cases where $w_d > b_{\text{fill}}$, the back circular segment became a half-circular segment, as shown in Fig. 4(b). Thus, the volume calculation became

$$V^*_{\text{fill}} = \alpha_{\text{fill}} = \frac{\pi}{8}b^{*2}_{\text{fill}} + \frac{\Lambda^2}{4}(\theta - \sin\theta) - \frac{h^*}{4}\left(1-\frac{\pi}{4}\right)(\pi b^*_{\text{fill}} + \Lambda\theta), \quad (5)$$

$$\theta = 2\arccos\left(1 - \frac{b^*_{\text{fill}}}{\Lambda}\right) \quad (6)$$

In these equations, the only unknown variable was the penetration depth b^*_{fill} at the end of the filling stage. Since the hydrodynamic force defines the final shape of the droplet, a mathematical expression for b^*_{fill} can be determined by force balance calculations, which are explained in the following sections.

C. Necking stage

In this stage, the droplet continues to grow as the neck of the droplet collapses. Therefore, the final droplet size depends on the shape of the droplet at this stage, the necking time and the flow rate ratios. The dimensionless necking time was defined as β in the current model, and it was correlated with the fraction of the flow of the continuous phase that was blocked by the interface. As the continuous phase pushed the interface to the opposite corner of the T junction, the shape of the fraction (control volume-red dashed area, see Fig. 5) changed. Once the neck reached the critical point ($2r^*_{\text{pinch}}$), the collapse of the droplet took place very fast. Thus, the shape of the fraction needed to be known to calculate the dimensionless necking time, β. Since the change in the control volume over time was related with the bypassing flow rate and squeezing flow rate of the continuous phase across the boundary of the droplet, dimensionless necking time was obtained by the following Eq. (7):

$$\beta = \left(V^*_{c_{\text{pinch}}} - \mathrm{V}^*_{c_{\text{fill}}}\right)\left(1-\frac{A^*_{\text{gap}}}{h^*}\right)^{-1}, \quad (7)$$

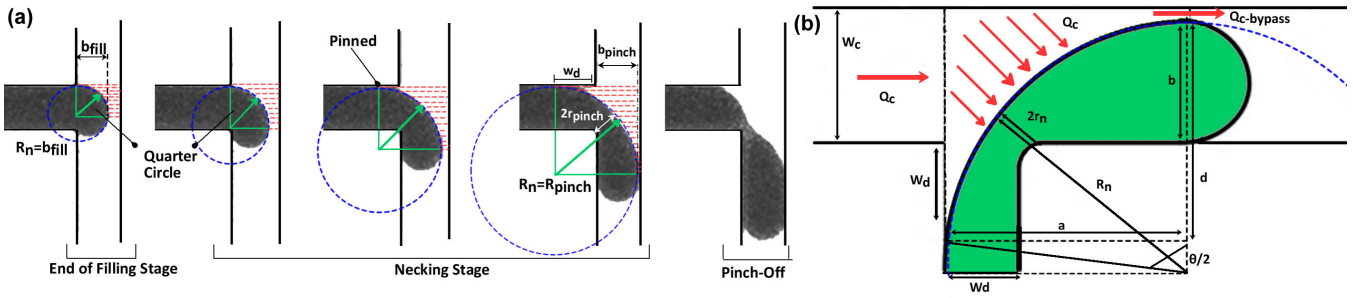

FIG. 5. (a) Sequence of microscopic images of the droplet during the necking stage showing elongation of the droplet and the transformation of the back half of the droplet from a quarter-circle to a circular-segment after the continuous phase pinned at a distance w_d. (b) Schematic of the droplet under the necking stage showing the required variables to calculate the volume of the droplet at this stage.

where $((1-({A_{\text{gap}}}^*)/h^*))^{(-1)}$ represents the fraction of the continuous phase that pushes the interface of the droplet to the opposite corner. The dimensionless bypass area, A^*_{gap} is defined by the following Eq. (8):

$$A^*_{\text{gap}} = (1-b^*_{\text{ave}})h^* + \left(1-\frac{\pi}{4}\right)\frac{h^{*2}}{2}. \tag{8}$$

Since the penetration depth is changing dynamically during the necking stage, the average penetration depth, $b^*_{\text{ave}} = (b^*_{\text{pinch}} + b^*_{\text{fill}})/2$ is used to define the gap. $V^*_{c_{\text{pinch}}}$ is the final dimensionless control volume at the pinch-off point, and $V^*_{c_{\text{fill}}}$ is the initial dimensionless control volume at the end of the filling stage. Both control volumes can be obtained by applying Eq. (1) to the two-dimensional (2D) shape of the droplet at those stages. $V^*_{c_{\text{fill}}}$ is given by Eq. (9):

$$V^*_{c_{\text{fill}}} = (1-b^*)R^*_{\text{fill}} + \left(1-\frac{\pi}{4}\right)(R^*_{\text{fill}})^2 + \frac{\pi h^*}{4}\left(1-\frac{\pi}{4}\right)R^*_{\text{fill}}. \tag{9}$$

In the model presented by van Steijn *et al.* for Newtonian fluids, the shape of the control volume at the pinch-off point is approximated as a quarter circle. However, it was found that due to the shear-thinning property of the blood solutions, the droplet elongated into the main channel before the detachment, and the quarter-circle shape was distorted. The distorted shape of the blood droplet presented a similar shape as that of a Newtonian liquid droplet formed under the transition regime [16,17]. The neck shape first followed a quarter-circle shape, and then was distorted as the continuous phase started to penetrate the dispersed phase channel, and became pinned at a distance, w_d. With the continuous phase becoming pinned in the dispersed phase channel, the droplet elongated into the main channel and the neck radius increased [$R^*_n = R^*_{\text{pinch}}$, see Figs. 5(a) and 5(b)]. As a result, the necking duration increased as the neck radius increased. Furthermore, unlike the droplets under the transition regime, it was found that as the oil viscosity increased, the elongation of the droplet increased, causing a larger neck radius. Thus, to develop a mathematical expression for $V^*_{c_{\text{pinch}}}$, a new description of the shape of the back of the droplet was implemented using the given variables in Fig. 5(b) and these variables were modified based on the shear-thinning property of the droplet:

$$d^* = b^*_{\text{pinch}} + \Lambda, \tag{10}$$

$$\theta = 2\arccos\left(1-\frac{\Lambda + b^*_{\text{pinch}}}{R^*_{\text{pinch}}}\right), \tag{11}$$

$$a^* = \eta\sqrt{d^*(2R^*_{\text{pinch}} - d^*)}, \tag{12}$$

$$2r^*_{\text{pinch}} - \varepsilon = R^*_{\text{pinch}} - \sqrt{(a^*-\Lambda)^2 + (R^*_{\text{pinch}} - b^*_{\text{pinch}})^2}, \tag{13}$$

where a^* is the elongation length, θ is the angle, ε is the roundness of the corner of the T junction and, η is the viscosity ratio of the phases. The roundness of the channel must be included to minimize the error (the corner of the T junction is always not perfectly 90 due to the fabrication). In shear thinning fluids (i.e., fluids with red blood cells), as the shear increases, the viscosity reduces, resulting in a dynamic viscosity rate ratio, η. However, the viscosity of the blood solutions varied only slightly under a wide range of shear rate. Therefore, the effect of the dynamic viscosity change was minimal, and the average viscosity value of the blood solutions calculated in this study provided enough accuracy for the analysis.

In the analysis of Glawdel *et al.* for droplet generation under the transition regime, it was shown that the shape of the droplet after the continuous phase penetrated the dispersed phase channel at a distance, w_d, was not a quarter circle [11]. Instead, the shape was a function of the critical neck thickness ($2r^*_{\text{pinch}}$), which depended on the viscosity ratio of the fluids and the channel geometry, for which an iterative approach using Eqs. (10)–(13) was taken to calculate R^*_{pinch} for a specific $2r^*_{\text{pinch}}$. However, our analysis showed that $2r^*_{\text{pinch}}$ was independent of the fluid viscosities and only changed when the aspect ratio of the channel was changed. The reason that a constant quarter-circle shape was not observed throughout the necking stage in our case was due to the elongation of the droplet. Therefore, the neck radius before pinch-off (R^*_{pinch}) was calculated by iterating the elongation length (a^*) of the droplet under different shear rates instead of $2r^*_{\text{pinch}}$. Hence, as the oil viscosity increased, the shear stress acting on the droplet increased resulting in a lower viscosity ratio, an elon-

gation of the droplet, and a larger neck radius R^*_{pinch}. This also explains why longer neck durations were observed under the more viscous continuous phases. After defining the back half of the droplet, the control volume at the pinch-off $V^*_{c_{\text{pinch}}}$ could be calculated by

$$V^*_{c_{\text{pinch}}} = (1 - {b_{\text{pinch}}}^*)a^* + (1-\Lambda)a^* - \left(\frac{{R^*_{\text{pinch}}}^2}{4}\right)(\theta - \sin\theta) + \frac{\theta h^*}{4}\left(1 - \frac{\pi}{4}\right)R^*_{\text{pinch}}. \quad (14)$$

As the final step, the calculated $V^*_{c_{\text{pinch}}}$ and $V^*_{c_{\text{fill}}}$ were substituted into Eq. (7) to determine β. In summary, α, φ, and β factors have been determined. However, there are still two mathematically undefined variables (b^*_{fill} and $2r^*_{\text{pinch}}$) exist. In the following section, these two quantities are defined.

D. Calculation of b^*_{fill} and $2r^*_{\text{pinch}}$

1. Force balance analysis of the emerging droplet

Droplet formation is governed by three major forces: interfacial tension force, viscous force, and pressure force. Once these forces are balanced, the characteristic shape of the droplet is formed. This point can be calculated by doing an overall force balance, and result in the penetration depth b^*_{fill}. The necking begins when the sum of the viscous shear and pressure forces exceed the interfacial tension force. Therefore, forces are required to be known to define the unknown penetration depth, b^*_{fill}.

The interfacial tension force resists the deformation of the emerging droplet. To calculate it, the projected area of the emerging droplet at the end of the filling stage is multiplied by the Laplace pressure difference between the upstream and downstream ends of the droplet. The curvature of the downstream end is $k_{\text{down}} = 2/b_{\text{fill}} + 2/h$; the upstream curvature is $k_{up} = 1/R_n + 2/h$, and, the projected area is approximated as $A \approx b_{\text{fill}}h$. The resulting interfacial tension force is thus given by Eq. (15):

$$F_\gamma \approx \left(-\gamma\left(\frac{2}{b_{\text{fill}}}+\frac{2}{h}\right)+\gamma\left(\frac{1}{R_{\text{n}}}+\frac{2}{h}\right)\right)b_{\text{fill}}h \approx -\gamma h. \quad (15)$$

The viscous force acts on the interface of the droplet to deform the droplet. The viscous force is given by the product of the shear stress acting on the droplet, and the associated area ($A \approx b_{\text{fill}}h$) on which that stress applies. The shear rate is approximated by the product of the continuous phase viscosity with the average velocity ($u_{\text{gap}} = Q_c/(w_c - b_{\text{fill}})$) of the continuous phase flowing through the gap $\tau \approx (\mu_c u_{\text{gap}})/h$ the the resulting viscous force is

$$F_\tau \approx \frac{\mu_C u_{gap}}{h} b_{\text{fill}}h \approx \frac{\mu_C Q_c}{h(w_c - b_{\text{fill}})} b_{\text{fill}}h \approx \frac{b_{\text{fill}}\ \mu_C Q_c}{(w_c - b_{\text{fill}})}. \quad (16)$$

The pressure force occurs due to the resistance of the dispersed phase to the flow of the continuous phase. As the dispersed phase blocks the interface, the resistance to the continuous phase flow increases and the pressure drops. Thus, the pressure force depends on the area $A \sim (b_{\text{fill}}h)$ of the given distance ($w_{\text{gap}} = w_c - b_{\text{fill}}$), and the magnitude of the pressure drop. The pressure drop can be approximated by using the lubrication analysis for pressure-driven flow in a thin-gap based on the Hagen-Poiseuille relation ($\Delta P = Q.\ R_{\text{hyd}}$) [3]. Q is the flow rate, $R_{\text{hyd}}(12\mu b_{\text{fill}}/(hw_{\text{gap}})^2)$ is the the hydraulic resistance of the channel, and ΔP ($Q_c 12\mu b_{\text{fill}}/(hw_{\text{gap}})^2$ is the pressure drop. Although this relationship is more complicated in the presence of non-Newtonian fluids, the current approximation provided enough information to determine the penetration depth at the end of the filling stage accurately. Based on this estimation, the resulting pressure force becomes

$$F_p \approx (\Delta PA) \approx \left(\frac{12\mu_C Q_c b_{\text{fill}}}{h^2(w_c - b_{\text{fill}})^2}\right)(b_{\text{fill}}h) \approx \frac{12\mu_C Q_c {b_{\text{fill}}}^2}{h(w_c - b_{\text{fill}})^2}. \quad (17)$$

It is noted that the viscous force is ∼0–5% of the pressure force ($\frac{F_\tau}{F_p}\frac{w_c - b_{fill}}{12 b_{fill}}$) and therefore it was neglected in order to develop a simpler equation for the penetration depth. Once the balance of these forces was achieved, a relationship between the penetration depth and the capillary number was obtained, which agrees with that presented by Christopher *et al.* [15].

$$\frac{1}{Ca} \approx \frac{{b_{fill}}^*}{(1 - {b_{fill}}^*)^3}. \quad (18)$$

The capability of the model to predict the penetration depth, Eq. (18) was validated by comparing the experimentally measured penetration depths across six cases that captured the influence of both geometric and flow conditions. Moreover, the penetration depths at a different capillary number of these six cases were included in the fitting. As shown in Fig. 6(a), fitting of the experimental data was satisfactory. Figure 6(b) presents the accuracy of the calculated penetration depth for all cases under the same flow rate ratios. Most of the data falls within an error range of ±10%. It should be noted that some error may be attributed to the measurement of variables during video analysis.

2. Laplace pressure balance of the emerging droplet

van Steijn *et al.* have demonstrated that the necking starts once the continuous phase bypassing the emerging droplet reverses direction due to the Laplace pressure difference from the tip and neck of the droplet. This additional flow speeds up the necking process, and pinch-off occurs immediately. Therefore, the critical neck thickness before pinch-off ($2r^*_{\text{pinch}}$) was defined by the Laplace pressures on both sides of the droplet. In this work, the definition of the Laplace pressures required slight modifications. The pressure at the neck of the droplet was defined as $P_{\text{neck}} = \gamma[1/R_n + 1/r_n,)]$ and the pressure at the tip of the droplet was defined as $P_{\text{tip}} = \gamma(2/h + 2/w_c)$. Once the sum of these forces equals zero, the flow reverses the direction, and the critical neck thickness is given by

$${2r_{pinch}}^* = \frac{h^*}{1 + h^*}. \quad (19)$$

The given expression suggests that the neck thickness was only a function of the channel geometry. The experimental data in part I presented a similar trend where the neck thickness was the function of the channel height only (see, Fig. 5 in part I). Calculated results from Eq. (19) were compared with six experimental cases spanning different Capillary numbers to predict the critical neck thickness. As shown in Fig. 7, the given expression agrees with the experimental data well,

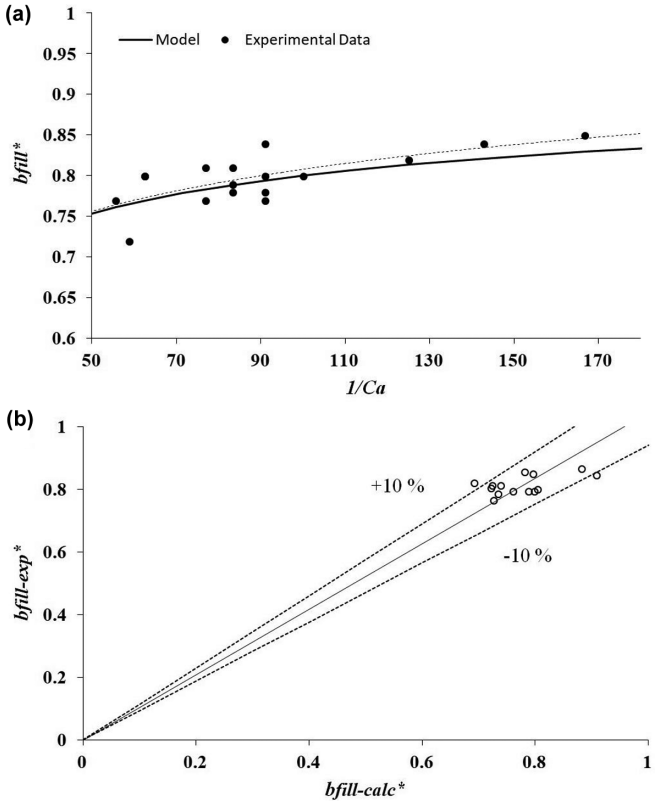

FIG. 6. Plots represents the performance of the model presented in Eq. (18). (a) Comparison of the experimental data with the model. The experimental data of six cases under different capillary numbers are fitted with the model developed during force balance analysis. (b) Parity plot of the penetration depth for all cases under the same flow rate ratio ∼0.04. The solid line represents the perfect parity, and the dashed lines are ±10%.

where all data falls into ±15%. Since pinch-off occurs suddenly, there is an error that comes in determining the exact frame of the pinch-off point.

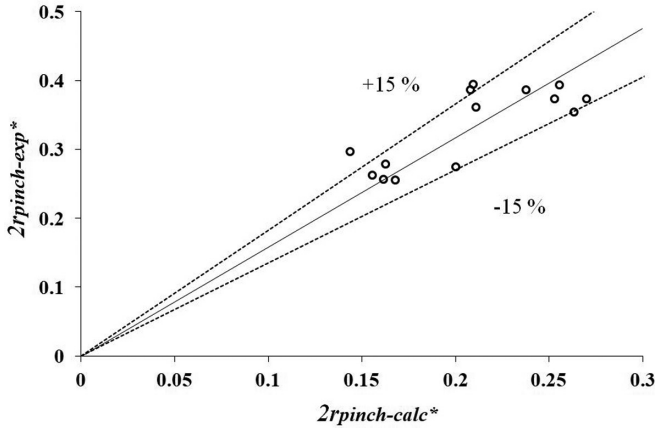

FIG. 7. The parity plot of critical neck thickness for all experiments under the flow rate ratio equals ∼0.04.

III. MODEL VALIDATION

Once the two variables b^*_{fill} and $2r^*_{\text{pinch}}$ were determined, by substituting these variables into Eqs. (4), (5), (13) the volume contributions of the filling (α_{fill}), and the necking stages ($\beta\varphi$) could be calculated. The volume contribution of the lag phase (α_{lag}) was only accounted for in the channel designs having a lower width ratio. For cases where $\Lambda = 0.5$, the final droplet volume was estimated using Eq. (1) ($V^*_d = \alpha_{\text{lag}} + \alpha_{\text{fill}} + \beta\varphi$). However, for the cases with $\Lambda = 1$, Eq. (1) was modified, and the final droplet volume was estimated without the contribution of lag phases ($V^*_d = \alpha_{\text{fill}} + \beta\varphi$). Validation of the

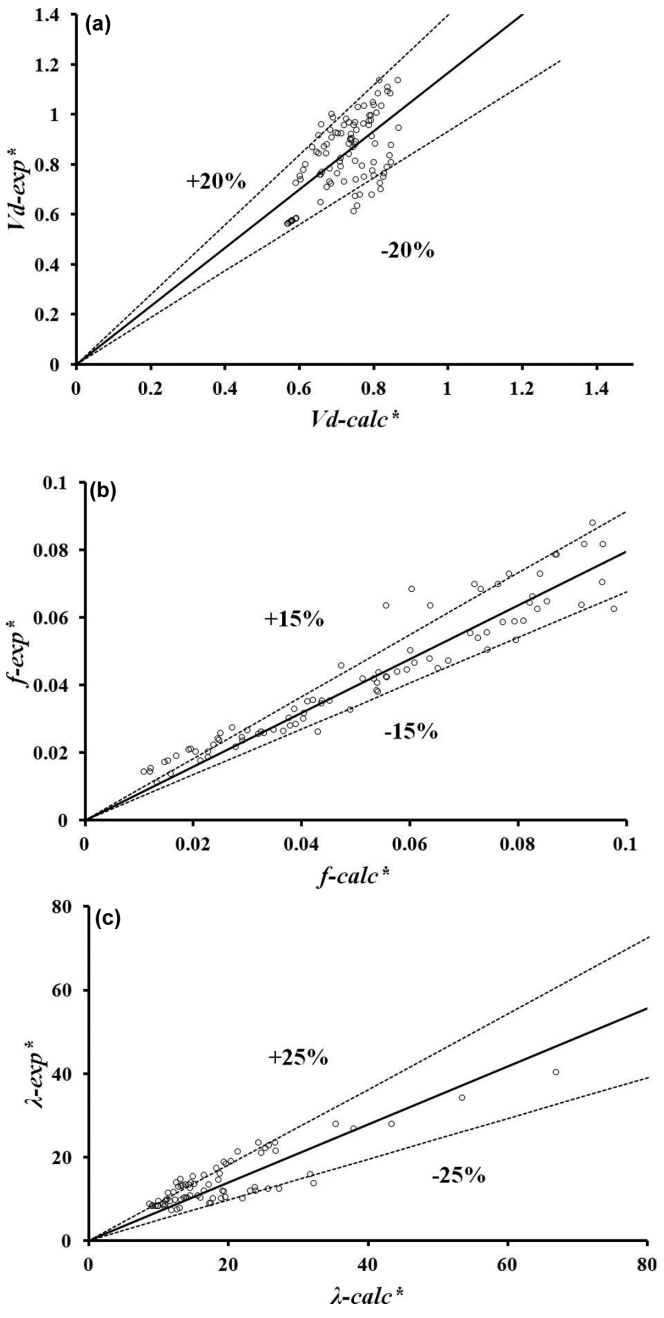

FIG. 8. Parity plots for model validation for three major operational parameters, (a) droplet volume, (b) droplet generation frequency, and (c) spacing between droplets for all experimental data.

physical model was analyzed using parity plots, as shown in Fig. 8(a). All the experimental data for T junctions $\Lambda = 0.5-1$ and $h^* = 0.4-0.6$ under conditions ranging from $\eta = 0.06-1$ and $Ca = 0.001-0.019$ fell within $\pm 20\%$. This suggests that the performance of the model was successful in predicting the final droplet volume formed in the T-junction generators under the squeezing regime.

The performance of the model was investigated on other operational parameters for the T-junction generator, such as spacing between droplets and generation frequency. The spacing between droplets, λ, was estimated by assuming that droplet length was proportional to the volume ($V_d^* \sim L_{\text{drop}}^*$):

$$\lambda = L_{\text{drop}} + L_c \approx \lambda^* = (\alpha_{\text{lag}} + \alpha_{\text{fill}})\left(\frac{\varphi + 1}{\varphi}\right) + (\varphi + 1)\beta. \tag{20}$$

The generation frequency was approximated using the reciprocal of the total generation time. The total formation was the sum of the duration of each stage $t^* = t_{\text{lag}}^* + t_{\text{fill}}^* + t_{\text{neck}}^*$ or

$$t^* = \frac{\alpha_{\text{lag}} + \alpha_{\text{fill}}}{\varphi} + \beta. \tag{21}$$

Rearranging to obtain the frequency yields

$$f^* = \frac{\varphi}{\alpha_{\text{lag}} + \alpha_{\text{fill}} + \beta\varphi}. \tag{22}$$

As shown in Figs. 8(b) and 8(c), the predictions for droplet spacing and generation frequency were in good correlation with the experimental data. We should note that the volume contribution of the lag phase was only included for $\Lambda = 0.5$ cases for both the spacing and the frequency calculations given in Eq. (20)–(22).

The discrepancies between the measured and model predicted frequency and spacing [Figs. 8(b) and 8(c)] come from the errors in image analysis and the model assumptions. During droplet volume calculation, it was assumed that the radius of the droplet curvature was half of the channel depth due to the unique droplet shape in the rectangular channel. The cross-sectional area, therefore, can be approximated as $A = wh - (1-\frac{\pi}{4})\frac{h^2}{2}$. To estimate the error in droplet volume, one can consider an extreme condition where the droplet fully touches the wall, and the cross-sectional area becomes $A = wh$. Then, for $h^* = 0.5$, the maximum error would be around 10.7%. However, the gutter regions of the channel provide more controlled wetting conditions, which reduces the error to ~2–5%. In addition, since the channel height is correlated with the penetration depth, the accuracy of the measured channel height highly influences the calculated volume results. Therefore, considering the listed error, the model fits well with the experimental results.

IV. CONCLUSION

In this second part of the two-part series, a physical model that describes the droplet formation of blood solutions in a T-junction generator under the squeezing regime was presented. The developed model can be utilized to predict the final droplet volume containing red blood cells. Since the major contributor of non-Newtonian behavior of blood is the red blood cell, the model can be extended to other blood solutions and similar biological non-Newtonian fluids based on the given channel geometry and flow conditions. The model was developed in three steps. First, the characteristic shape of the blood droplet at the end of the filling stage and during the necking stage was determined. Then, force and Laplace pressure balances were performed to define the penetration depth, b_{fill}^* and the pinch-off point, $2r_{\text{pinch}}^*$, which were substituted into the volume calculations of the droplet at the filling and necking stages. Finally, the experimental data was compared with the model predictions. It was shown that the model's predictions are in good agreement with the experimental data for various conditions such as different the flow rate ratios, viscosity ratios, blood cell concentrations, channel geometries, and capillary numbers.

[1] M. Marcali, X. Chen, M. G. Aucoin, and C. L. Ren, Droplet formation of biological non-Newtonian fluid in T-junction generators. I. Experimental investigation, Phys. Rev. E **105**, 025105 (2022).

[2] B. Steinhaus, A. Q. Shen, and R. Sureshkumar, Dynamics of viscoelastic fluid filaments in microfluidic devices, Phys. Fluids **19**, 073103 (2007).

[3] G. F. Christopher and S. L. Anna, Microfluidic methods for generating continuous droplet streams, J. Phys. D. Appl. Phys. **40**, R319 (2007).

[4] J. Husny and J. J. Cooper-White, The effect of elasticity on drop creation in T-shaped microchannels, J. Non-Newton. Fluid Mech. **137**, 121 (2006).

[5] Q. Zhang, C. Zhu, W. Du, C. Liu, T. Fu, Y. Ma, and H. Z. Li, Formation dynamics of elastic droplets in a microfluidic T-junction, Chem. Eng. Res. Des. **139**, 188 (2018).

[6] X. Sun, C. Zhu, T. Fu, Y. Ma, and H. Z. Li, Breakup dynamics of elastic droplet and stretching of polymeric filament in a T-junction, Chem. Eng. Sci. **206**, 212 (2019).

[7] B. Rostami and G. L. Morini, Experimental characterization of a micro cross-junction as generator of newtonian and non-newtonian droplets in silicone oil flow at low capillary numbers, Exp. Therm. Fluid Sci. **103**, 191 (2019).

[8] J. S. Horner, M. J. Armstrong, N. J. Wagner, and A. N. Beris, Investigation of blood rheology under steady and unidirectional large amplitude oscillatory shear, J. Rheol. **62**, 577 (2018).

[9] V. van Steijn, C. R. Kleijn, and M. T. Kreutzer, Predictive model for the size of bubbles and droplets created in microfluidic T-junctions, Lab Chip **10**, 2513 (2010).

[10] See Supplemental Material at http://link.aps.org/supplemental/10.1103/PhysRevE.105.025106 for the summary of variables, parameters and equations involved in this study.

[11] T. Glawdel and C. L. Ren, Droplet formation in microfluidic T-junction generators operating in the transitional regime. III. dynamic surfactant effects, Phys. Rev. E **86**, 026308 (2012).

[12] A. Günther and K. F. Jensen, Multiphase microfluidics: From flow characteristics to chemical and materials synthesis, Lab Chip **6**, 1487 (2006).

[13] M. L. J. Steegmans, A. Warmerdam, K. G. P. H. Schroen, and R. M. Boom, Dynamic interfacial tension measurements with microfluidic Y-junctions, Langmuir **25**, 9751 (2009).

[14] K. Wang, Y. C. Lu, J. H. Xu, and G. S. Luo, Determination of dynamic interfacial tension and its effect on droplet formation in the T-shaped microdispersion process, Langmuir **25**, 2153 (2009).

[15] G. F. Christopher, N. N. Noharuddin, J. A. Taylor, and S. L. Anna, Experimental observations of the squeezing-to-dripping transition in T-shaped microfluidic junctions, Phys. Rev. E **78**, 036317 (2008).

[16] T. Glawdel, C. Elbuken, and C. L. Ren, Droplet formation in microfluidic T-junction generators operating in the transitional regime. I. experimental observations, Phys. Rev. E **85**, 016322 (2012).

[17] T. Glawdel, C. Elbuken, and C. L. Ren, Droplet formation in microfluidic T-junction generators operating in the transitional regime. II. modeling, Phys. Rev. E **85**, 016323 (2012).